

Access Zone Luminance Prediction for a Road Tunnel under a Cloudless Sky

Wei He^{1,2} and Bo Liang^{1,*}

¹School of Civil Engineering, Chongqing Jiaotong University, Chongqing 400074, China

²Department of Traffic and Municipal Engineering, Sichuan College of Architectural Technology, Chengdu 610399, China

Received 3 August 2021; Accepted 29 October 2021

Abstract

Access zone luminance is affected by many factors, such as weather, test time, the location of the tunnel, the inclination of the portal, the orientation of the portal, and the colors of objects outside the tunnel. It is considerably difficult to predict. In order to predict access zone luminance under a cloudless sky accurately, the model for object surface luminance was proposed. The law about ratio of the normal luminance to the illuminance on the object surface was found through measurement. The influence of viewing angle on the luminance of a typical object outside the tunnel was analyzed. The predicted object surface luminance and access zone luminance were verified using the corresponding measured values, and the reasons for prediction error were analyzed. Results show that the daylight received by an object within a 20-degree field of view is approximately uniformly reflected in all directions. The ratio of luminance to illuminance on the surface of the object with a specific color can be supposed as constant when predicting access zone luminance. The proposed access zone luminance prediction method under a cloudless sky has good versatility, and the input parameters of the prediction method include all factors that affect access zone luminance. The relative root-mean-square error and relative mean bias error of the predicted access zone luminance in the case are 11.6% and 11.4%, respectively. This study provides a reference for intelligent dimming of highway tunnel lighting.

Keywords: Illuminance, Luminance, Field of view, Tunnel

1. Introduction

Daylight can reduce the lighting demand of buildings[1]; however, it increases the need for tunnel lighting. When a driver passes into a tunnel rapidly during the daytime, the human eyes cannot adapt to the sharp change in luminance between inside and outside the tunnel, and temporary blindness will occur. The difference between access zone luminance (L_{20}) and threshold zone luminance should be reduced to prevent this situation. Therefore, the International Commission on Illumination (CIE) proposed that the threshold zone in a tunnel should be equipped with enhanced lighting whose luminance is a certain ratio of access zone luminance. The transition zone lighting level should decrease gradually to make the human eyes gradually adapt from the high-illuminated threshold zone to the darker interior zone, and transition zone luminance is determined by L_{20} . Given that the luminance of the threshold and transition zones is much greater than that of the interior zone, the entire tunnel lighting energy consumption is concentrated in the threshold and transition zones (except for an ultralong tunnel). Thus, L_{20} is an important parameter that determines the daily operating costs of tunnel lighting and the investment in lighting equipment.

CIE defines L_{20} as the average luminance of a tunnel entrance seen by a driver at a specific point, which is located at the center of lanes, at the height of 1.5 m, and at a distance from the tunnel portal equal to the stopping distance. The average luminance is taken from a 20-degree conical field of view, which is centered on one-quarter the height of the

tunnel opening.

The traditional tunnel lighting design determines the installed power of lamps in accordance with the maximum L_{20} (cumulative frequency) in a year. With the maximum L_{20} as the basis for tunnel lighting operation, tunnels are often overlit. With the maturity of adjustable LED and intelligent control technology, the luminance of the threshold and transition zones can be adjusted in real time in accordance with L_{20} , which realizes energy saving in the tunnel while ensuring driving safety. The premise of tunnel intelligent dimming is that L_{20} can be rapidly predicted. However, many influencing factors exist for L_{20} , which causes great difficulties in the prediction of L_{20} .

On this basis, scholars have conducted studies on the influence of landscape color, portal orientation, the percentage of objects in the 20-degree field of view, and test time on L_{20} [2-6]. Nevertheless, studies in the past were still at the stage of qualitative analysis, and no L_{20} prediction model had been established. Therefore, accurately predicting L_{20} and clarifying the functional relationship of L_{20} with weather, test time, the location of the tunnel, the inclination angle of the tunnel portal, the tunnel portal orientations, the color of objects, and the percentage of objects are pressing issues.

To this end, this study used theoretically calculated global illuminance received by an object to predict the object surface luminance and then obtained the predicted L_{20} , providing a reference for intelligent dimming of tunnel lighting.

*E-mail address: liangbo_laoshi@163.com

ISSN: 1791-2377 © 2021 School of Science, IHU. All rights reserved.

doi:10.25103/jestr.145.06

2. State of the art

CIE first proposed the use of a luminance meter with a 20-degree viewing angle to measure L_{20} in 1984. In 1990, it clarified the definition and the determination method for L_{20} . In 2004, the perceived contrast method was proposed, while L_{20} method was kept in annexes. Many scholars have conducted related studies on L_{20} and the luminance of landscape around the entrance portal. Gueorgiev[7] proposed that a high L_{20} value causes the energy consumption of tunnel lighting during the day in summer to be 9 times that of at night. Peña-García et al.[8] proposed that coefficient k , the length of threshold and transition zones, and L_{20} are minimized by restricting the maximum speed of road tunnels, resulting in a reduction in tunnel energy consumption and the number of lamps, but they did not mention the disadvantages of the above method. Onaygil et al.[2] presented measures to reduce L_{20} , such as rough and dark surfaces of tunnel portals, road paving, high retaining walls, and green plants, trees, and shrubs around the tunnel, to achieve the purpose of an energy-saving tunnel, but many conclusions of the study were based on computer simulations rather than measured data. García-Trenas et al.[3] suggested measures to decrease L_{20} , including planting low-reflectivity ivy around the tunnel entrance in different climates, such as the Alps and the Mediterranean, and installing colored panels with simulated vegetation patterns to block the sky in the 20-degree field of view. In spite of this, ivy was not tested in other climates, and the species characteristics that were most suitable for tunnels in other climates were not determined. Peña-García et al.[9] proposed to install black solar panels around a tunnel, which not only provides power for the tunnel facilities (lighting, ventilation, emergency) but also reduces L_{20} , which significantly saves energy consumption, carbon dioxide emissions, and investment in lighting installations. However, no profit algorithm for installing solar panels based on the direction of the tunnel and the surrounding terrain was developed. López et al.[10] presented that when the lamps of an open traffic tunnel need to be updated or maintained, vehicle-based images can be used to obtain L_{20} , without the need to take photos from the stopping distance to improve test safety, but the study ignored that objects in the 20-degree field of view of a driver may be different for various distances. Blaser et al.[11] proposed that the safe maximum L_{20} be obtained from the cumulative frequency distribution of L_{20} throughout a year on the basis of the known empirical relationship between luminance and daylight illuminance and the average relative sunshine time distribution in the relevant area during a year, but the proposed method had poor accuracy. Pachamanov et al.[12] obtained the safe maximum L_{20} with different orientations of the entrance portal in Bulgaria. Doulos et al.[13] calculated L_{20} in 11 existing tunnels and used the traffic weighting method to calculate threshold zone luminance, thereby reducing the luminance curve of the transition zone. Nonetheless, the proposed method was not combined with traffic detection sensors because the traffic volume can determine tunnel class and thus the lighting needs. Bouroussis et al.[4] investigated that the lateral position of L_{20} instrument would cause a 20-degree field of view

difference between a driver and the instrument and studied the effect of the field of view difference on L_{20} for different orientations. However, the study only considered four orientations, i.e., east, west, south, and north; more orientations were not studied. Xu et al.[14] introduced the research idea of the dynamic characteristics of access zone luminance and believed that the dynamic change of access zone luminance is essentially formed by the change in the illuminance received by objects outside a tunnel, but the law of dynamic change of access zone luminance was not studied. Zhao et al.[5, 6] analyzed the changing law of L_{20} with time under different tunnel portal orientations. Nevertheless, they did not study the changing law of L_{20} with tunnel portal orientations and weather. Deng et al.[15] established the relationship between the luminance of landscape outside a tunnel and horizontal illumination through measurements and proposed a new method to determine the luminance of landscape outside the tunnel. Zhang[16] used the radiation data of a weather station and an established irradiance–illuminance conversion model to obtain vertical illuminance, then the luminance of scenery around a tunnel was determined in combination with the reflection coefficient. He et al.[17] used an SLR digital camera to test L_{20} and improved a post-processing method for L_{20} . The proposed post-processing method increased the efficiency by more than 10 times, and the accuracy of L_{20} was also increased. Nevertheless, the digital camera was only calibrated outdoors with a luminance meter, without using a better integrating sphere. Xiao[18] used an OV5640 camera calibrated with an imaging photometer to measure L_{20} , and a set of Linux-based luminance measurement systems was developed. Liang et al.[19] proposed that global horizontal irradiance and illuminance under a cloudless sky are linear functions of solar altitude angle, and a slope illuminance prediction method that does not rely on measured data was developed, laying the foundation for L_{20} prediction under a cloudless sky. However, the proposed method only verified the predicted illuminance in mild climate zones, and the performance of the proposed method in polar, cold, arid, and equatorial climate zones was not studied.

The above analyses conducted studies on minimizing L_{20} , measuring L_{20} , and obtaining the safe maximum L_{20} . Nonetheless, few studies exist on the prediction of L_{20} . The ratio of luminance to illuminance of a specific color object within a 20-degree field of view is an approximate constant. The global illuminance received by an object is predicted first, then the object surface luminance is calculated. L_{20} is predicted last in accordance with the percentage of objects in the 20-degree field of view. The predicted object surface luminance and L_{20} are verified with the measured values, and the reasons for errors for predicting L_{20} are analyzed.

The rest of this study is organized as follows. The third section establishes L_{20} forecasting method system. The fourth section verifies the predicted values through measurements. The fifth section draws the conclusion of this study.

3. Methodology

3.1 Prediction of solar position

Daylight includes direct sunlight and sky light. Objects outside a tunnel reflect daylight to form object luminance. The average object luminance in the 20-degree field of view received by a driver at the stopping distance outside the tunnel is L_{20} . The solar position (the solar elevation, zenith, and azimuth) should be obtained to predict L_{20} . The solar altitude angle is obtained using the following formula (1)[20]:

$$A_{as} = \frac{180}{\pi} \arcsin(\sin l_a \sin D_s + \cos l_a \cos D_s \cos A_{is}) \quad (1)$$

where A_{as} is the angle of elevation of the sun above the horizon (degrees); π is the pi; l_a is the geographic latitude (degrees), D_s is the sun declination angle (degrees), which is calculated using Formula (2); and A_{is} is the solar hour angle (degrees), which is expressed in Formula (5).

$$D_s = 0.3723 - 0.758 \cos \bar{\mathcal{U}} + 0.3656 \cos(2\bar{\mathcal{U}}) + 0.0201 \cos(3\bar{\mathcal{U}}) + 23.2567 \sin \bar{\mathcal{U}} + 0.1149 \sin(2\bar{\mathcal{U}}) - 0.1712 \sin(3\bar{\mathcal{U}}) \quad (2)$$

where $\bar{\mathcal{U}}$ (radians) is calculated as

$$\bar{\mathcal{U}} = 0.0172(N_x - N_2) \quad (3)$$

where N_x is the day of a year (dimensionless). For example, February 1 is the 32nd day of the year, that is, $N_x = 32$.

$$N_2 = 0.2422y - 401.0906 - \text{INT}\left(\frac{y-1985}{4}\right) \quad (4)$$

where y represents the year, and INT is a function that returns an integer.

The solar hour angle is expressed as follows:

$$A_{is} = 15t_s - 180 \quad (5)$$

where t_s is the solar time (hours), which is obtained as

$$t_s = \begin{cases} t_{loc} + \frac{15|z_t| - L_{loc}}{15} + \mathcal{G} & \text{Western Hemisphere} \\ t_{loc} - \frac{15|z_t| - L_{loc}}{15} + \mathcal{G} & \text{Eastern Hemisphere} \end{cases} \quad (6)$$

where t_{loc} is the local standard time (hours), z_t is the time zone (dimensionless), and L_{loc} is the local longitude (degrees).

$$g = \frac{0.0028 - 1.9857 \sin \bar{\mathcal{U}} + 9.9059 \sin(2\bar{\mathcal{U}}) - 7.0924 \cos \bar{\mathcal{U}} - 0.6882 \cos(2\bar{\mathcal{U}})}{60} \quad (7)$$

The angular distance between the sun and zenith A_{zs} (radians) is expressed as follows:

$$A_{zs} = \frac{\pi}{2} - \frac{\pi}{180} A_{as} \quad (8)$$

The azimuth of the sun (clockwise from the north) is obtained using the following formula[20]:

$$AZ_s = \begin{cases} \pi - \arccos \frac{\sin A_{as} \sin l_a - \sin D_s}{\cos A_{as} \cos l_a} & t_s \leq 12 \\ \pi + \arccos \frac{\sin A_{as} \sin l_a - \sin D_s}{\cos A_{as} \cos l_a} & t_s > 12 \end{cases} \quad (9)$$

where AZ_s is the azimuth of the sun (radians).

3.2 Prediction of global illuminance received by an object

The global illuminance received by an object is an important physical quantity for predicting L_{20} , which is expressed as follows:

$$I_{\beta g} = I_{\beta d} + I_{\beta s} + I_{\beta r} \quad (10)$$

where $I_{\beta g}$ is the global illuminance received by the object (lux), $I_{\beta d}$ is the diffuse illuminance received by the object (lux), $I_{\beta s}$ is the direct illuminance received by the object (lux), and $I_{\beta r}$ is the reflected illuminance received by the object (lux).

$I_{\beta d}$ is calculated using the Perez model[21, 22], which is the point source simplified version, as shown as follows:

$$I_{\beta d} = I_{hd} [0.5(1 + \cos \beta)(1 - F_s) + F_s(a/b) + F_h \sin \beta] \quad (11)$$

where I_{hd} is the diffuse illuminance in the horizontal plane (lux); β is the inclination angle of the object surface (degrees); F_s and F_h are the anisotropy coefficients (dimensionless) of circumsolar and the horizon, respectively, which are expressed in Formulas (18) and (19). The calculations of a and b are shown in Formulas (25) and (26).

$$I_{hd} = I_{hg} - I_{is} \sin A_{as} \quad (12)$$

where I_{hg} is the global illuminance in the horizontal plane (lux), and I_{is} is the normal incidence direct illuminance (lux). Under a cloudless sky, I_{hg} is expressed as follows[19]:

$$I_{hg} = 1486.667 A_{as} \quad (13)$$

I_{is} is obtained using the following formula[23]:

$$I_{is} = I_{ex} \cdot f_c \cdot \exp(-m \cdot f_e \cdot f_l) \quad (14)$$

where I_{ex} is the extraterrestrial illuminance, which is 133800 lux. f_c is the date correction (dimensionless) of extraterrestrial illuminance constant, m is the relative air mass (dimensionless), and f_e is the luminous extinction (dimensionless) under dry and clean air, which are expressed in Formulas (15)[24], (16)[25], and (17)[25], respectively. f_l is the luminous turbidity factor (dimensionless). For a cloudless sky, the value of f_l is 2.5[26].

$$f_c = 1 + 0.0337 \cos[0.9863(N_x - 4)] \quad (15)$$

$$m = \frac{1}{\sin A_{as} + 0.50572(A_{as} + 6.07995)^{-1.6364}} \quad (16)$$

$$f_e = \frac{1}{10.1 + 0.045m} \quad (17)$$

F_s and F_h in Formula (11) are expressed as

$$F_s = f_{s1} + f_{s2}\Delta + f_{s3}A_{zs} \quad (18)$$

$$F_h = f_{h1} + f_{h2}\Delta + f_{h3}A_{zs} \quad (19)$$

where f_{s1} , f_{s2} , f_{s3} , f_{h1} , f_{h2} , and f_{h3} are the illuminance coefficients (dimensionless) of the point source simplified Perez model, as shown in Table 1.

Table 1. Illuminance coefficients of the point source simplified Perez model

ε	Upper bound	f_{s1}	f_{s2}	f_{s3}	f_{h1}	f_{h2}	f_{h3}
1	1.065	0.011	0.57	-0.081	-0.095	0.158	-0.018
2	1.23	0.429	0.363	-0.307	0.05	0.008	-0.065
3	1.5	0.809	-0.054	-0.442	0.181	-0.17	-0.092
4	1.95	1.014	-0.252	-0.531	0.275	-0.35	-0.096
5	2.8	1.282	-0.42	-0.689	0.38	-0.56	-0.114
6	4.5	1.426	-0.653	-0.779	0.425	-0.79	-0.097
7	6.2	1.485	-1.214	-0.784	0.411	-0.63	-0.082
8	—	1.17	-0.3	-0.615	0.518	-1.89	-0.055

The brightness of the sky (dimensionless), Δ , is defined as

$$\Delta = \frac{mE_{hd}}{E_{ex}} \quad (20)$$

where E_{hd} is the diffuse irradiance in the horizontal plane (W/m^2); and E_{ex} is the extraterrestrial irradiance, which is $1366 W/m^2$.

$$E_{hd} = E_{hg} - E_{is} \sin A_{as} \quad (21)$$

where E_{hg} is the global irradiance in the horizontal plane (W/m^2); under a cloudless sky, it can be obtained using Formula (22)[19]. E_{is} is the normal incidence direct irradiance (W/m^2), and it can be obtained using Formula (23) under a cloudless sky[27].

$$E_{hg} = 15.178A_{as} \quad (22)$$

$$E_{is} = 1353 * 0.7^m \quad (23)$$

The clearness of the sky (dimensionless) in Table 1., ε , is defined as

$$\varepsilon = \frac{1.041A_{zs}^3 + \frac{E_{is} + E_{hd}}{E_{hd}}}{1 + 1.041A_{zs}^3} \quad (24)$$

a and b in Formula (11) are expressed as follows:

$$a = \max(0, \cos A_{\beta i}) \quad (25)$$

$$b = \max(0.087, \cos A_{zs}) \quad (26)$$

where $A_{\beta i}$ is the angle of incidence on the object surface, and it is obtained as follows:

$$\cos A_{\beta i} = \sin A_{as} \cos \beta + \cos A_{as} \sin \beta \cos(\psi - AZ_s) \quad (27)$$

where ψ is the azimuth (radians) that the object surface faces.

The direct illuminance received by the object is determined by I_{is} and $A_{\beta i}$, as shown as follows:

$$I_{\beta s} = I_{is} \cos A_{\beta i} \quad (28)$$

The reflected illuminance received by the object is expressed as

$$I_{\beta r} = 0.5f_g I_{hg} (1 - \cos \beta) \quad (29)$$

where f_g is the albedo coefficient (dimensionless). In the absence of measured data, the value of f_g is 0.2[28].

3.3 Proposed prediction model for object surface luminance

Assuming that the daylight received by objects within a 20-degree field of view is uniformly reflected in all directions, the ratio of luminance to illuminance of a specific color object is constant, and this ratio is denoted as r . This law will be confirmed in Section 4. The luminance of the object can be expressed as

$$L = I_{\beta g} \cdot r \quad (30)$$

where L is the object surface luminance.

3.4 Proposed prediction model for L_{20}

In consideration of the different colors of objects in the 20-degree field of view, this field of view is divided into n regions, then L_{20} is expressed as follows:

$$L_{20} = \sum_{i=1}^{i=n} L_i p_i \quad (31)$$

where L_i is the luminance of the i -th color object, and p_i is the percentage of the i -th color object in the 20-degree field of view.

$$p_1 + p_2 + \dots + p_n = 1 \quad (32)$$

The above 32 formulas should be programmed to improve the prediction efficiency of L_{20} . The input

parameters of the prediction L_{20} program include the test date, t_{loc} , z_t , L_{loc} , I_a , β , ψ , r , and p_i . The above input parameters are all factors that affect L_{20} . Therefore, all influencing factors have been quantified in the proposed L_{20} prediction method.

4 Result Analysis and Discussion

4.1 Ratio of normal luminance to illuminance

Normal luminance and illuminance on object surface were tested. The tested objects included a horizontal asphalt pavement and vertical cards made of tender green and dark green leaves. The test site was located at 104.41 degrees east longitude and 31.09 degrees north latitude. The luminance meter (LS-150, Konica Minolta, Tokyo, Japan) and illuminance meter (TES-1339R, TES Electrical Electronic Corp., Taipei, Taiwan) were calibrated before use. The results in Tables 2–4 show that the ratio of normal luminance to illuminance on the surface of a specific color object is approximately constant. The test time and weather do not affect this ratio, but the object color is the decisive factor for this ratio.

Table 2. Ratio of normal luminance to illuminance on a horizontal asphalt pavement

Date	Time	Weather	L_{Rn} (cd/m ²)	I_R (lux)	$\frac{L_{Rn}}{I_R}$ (cd/lm)
5/27/2020	9:35	Overcast	310.2	4136	0.075
	10:22		398.7	5462	0.073
	11:23		527.1	7123	0.074
	12:45		661.0	9180	0.072
	13:10		685.4	9019	0.076
	14:20		794.2	11680	0.068
	15:15		500.8	7475	0.067
5/29/2020	8:49	Clear	3567	50240	0.071
	9:49		5128	69300	0.074
	10:50		6380	88610	0.072
	11:50		7682	106700	0.072
	12:59		8259	119700	0.069
	13:31		8606	116300	0.074
	14:29		7366	100900	0.073
	15:35		5713	80470	0.071
	16:44		4273	58540	0.073

L_{Rn} and I_R are the normal luminance and illuminance on a horizontal asphalt pavement, respectively.

Table 3. Ratio of normal luminance to illuminance on a vertical card made of a tender green leaf

Date	Time	Weather	L_{TGvn} (cd/m ²)	I_{TGv} (lux)	$\frac{L_{TGvn}}{I_{TGv}}$ (cd/lm)
12/24/2020	14:45	Overcast	511.2	8960	0.057
	15:27		293.8	5890	0.050
	15:45		256.1	4648	0.055
	16:17		206.2	3656	0.056
	16:39		136.7	2673	0.051
	17:07		106.3	2139	0.050
	17:27		96.13	1757	0.055
12/23/2020	13:36	Clear	979.4	18480	0.053
	14:00		1368	26820	0.051
	14:25		1960	35000	0.056
	14:52		2277	42960	0.053
	15:16		2544	48930	0.052
	15:46		2867	54100	0.053

16:28	2752	53970	0.051
17:05	2231	41310	0.054

L_{TGvn} and I_{TGv} are the normal luminance and illuminance on a vertical card made of a tender green leaf, respectively.

Table 4. Ratio of normal luminance to illuminance on a vertical card made of a dark green leaf

Date	Time	Weather	L_{DGvn} (cd/m ²)	I_{DGv} (lux)	$\frac{L_{DGvn}}{I_{DGv}}$ (cd/lm)
12/24/2020	14:35	Overcast	100.6	5826	0.017
	15:05		84.13	5162	0.016
	15:37		58.88	3324	0.018
	16:00		52.97	3228	0.016
	16:27		53.48	2933	0.018
	17:00		41.19	2247	0.018
12/23/2020	17:17	Clear	39.06	2197	0.018
	13:46		1323	77850	0.017
	13:58		1310	77040	0.017
	14:11		1215	75950	0.016
	14:34		1324	73570	0.018
	15:02		1184	69650	0.017
	15:18		1137	66860	0.017
	15:28		1103	64890	0.017
	15:42		1113	61820	0.018
	15:56		990.9	58290	0.017
	16:11		862.1	53880	0.016
16:39	735.6	43270	0.017		
17:15	417.5	24560	0.017		

L_{DGvn} and I_{DGv} are the normal luminance and illuminance on a vertical card made of a dark green leaf, respectively.

4.2 Effect of viewing angle on object surface luminance

In the 20-degree field of view, a driver's eyes receive object surface luminance, which is at different viewing distances and angles. Given that the viewing distance does not affect object surface luminance, the object surface luminance at different viewing angles was studied. Both LS-150 luminance meters measured an object's luminance at the same time, one of which measured the normal luminance (0-degree viewing angle), and the other one measured the luminance at a 72-degree viewing angle. The luminance on a horizontal asphalt pavement, a vertical card made of a tender green leaf, and a vertical card made of a dark green leaf at a 72-degree viewing angle are denoted as L_{R72} , L_{TGv72} , and L_{DGv72} , respectively. Figures 1–3 demonstrate that the luminance at the 72-degree viewing angle is close to its normal luminance. Figures 4–6 show that the relative error between the luminance at the 72-degree viewing angle and its normal luminance is -10%–4% and 4%–10%. This relative error exceeds ±2%, which is the uncertainty of the LS-150 luminance meter, such that the luminance difference at different viewing angles is not caused by the measurement error of the LS-150 luminance meter. Therefore, the tested objects reflect daylight approximately evenly in all directions. To simplify the prediction of L_{20} , it is necessary to assume that the luminance of an object within the 20-degree field of view is the same at all viewing angles. Given that the ratio of normal luminance to the illuminance on the surface of a specific color object is approximately a fixed value, it can be assumed that the ratio of luminance to the illuminance on the surface of a specific color object at any viewing angle is constant when predicting L_{20} .

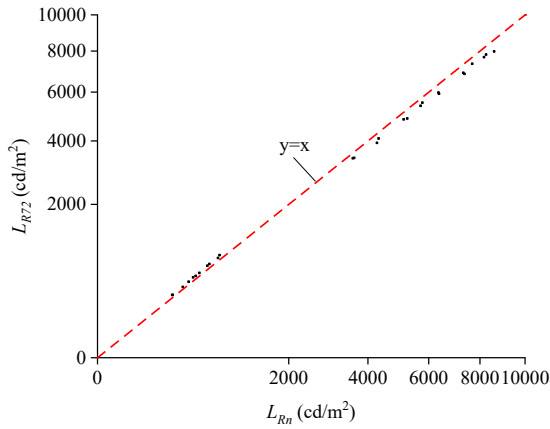


Fig. 1. Scatterplot of L_{Rn} vs. L_{R72}

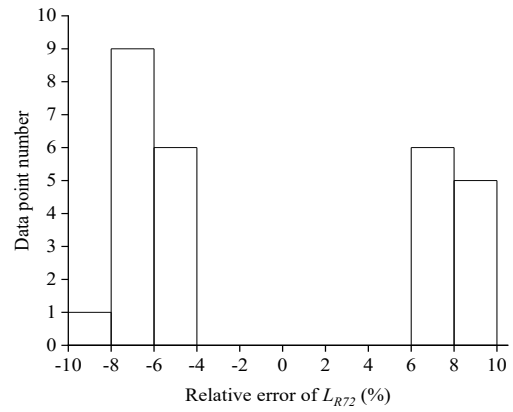


Fig. 4. Relative error histogram of L_{R72}

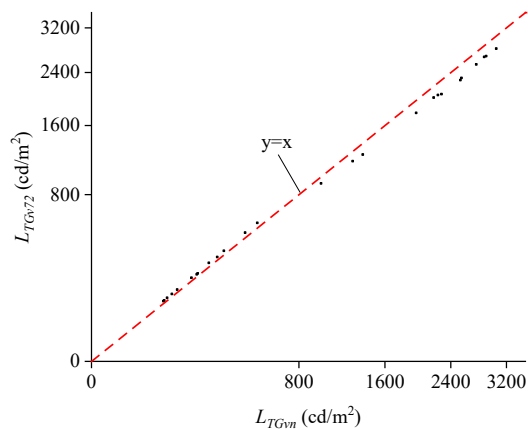


Fig. 2. Scatterplot of L_{TGvn} vs. L_{TGv72}

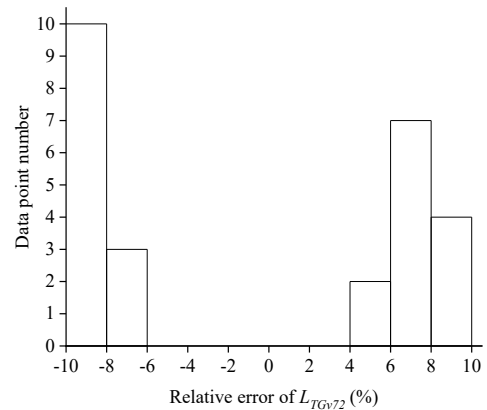


Fig. 5. Relative error histogram of L_{TGv72}

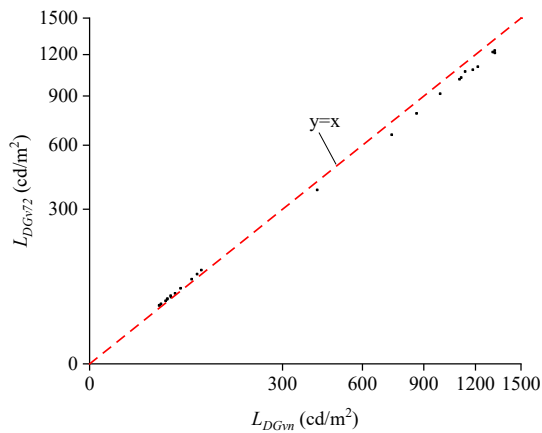


Fig. 3. Scatterplot of L_{DGvn} vs. L_{DGv72}

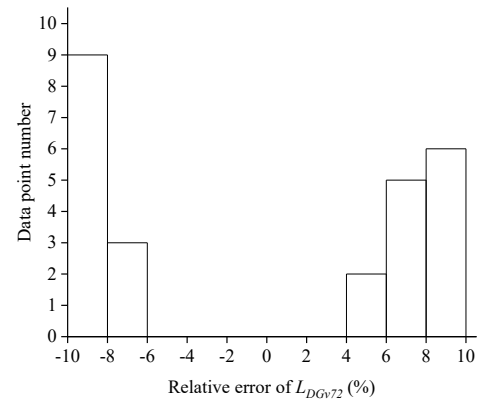


Fig. 6. Relative error histogram of L_{DGv72}

4.3 Object surface luminance verification

Object surface luminance is the basis for predicting L_{20} . In this study, the luminance of the horizontal asphalt pavement and the vertical cards facing east, west, south, and north was measured every 10 min. The cards were made of tender green leaves. The above five luminance are denoted as L_R , L_{TGev} , L_{TGvn} , L_{TGsv} , and L_{TGnv} , respectively. The test site was located at 104.41694 degrees east longitude and 31.09056 degrees north latitude. The test time was 10:45–14:55 on July 2, 2020. The sky was cloudless during the test. Figures 7–11 show the comparison results of the measured and predicted values of object surface luminance. The predicted luminance is close to the measured values, except for L_{TGnv} .

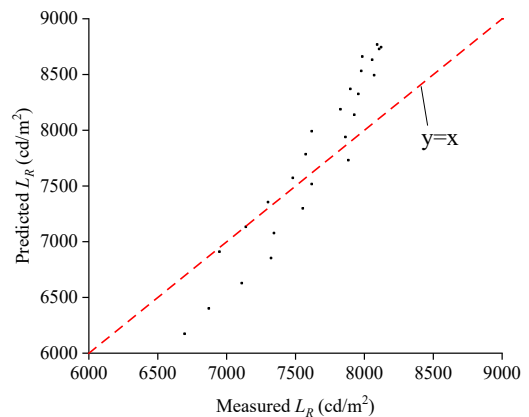


Fig. 7. Scatterplot of the measured L_R vs. the predicted L_R

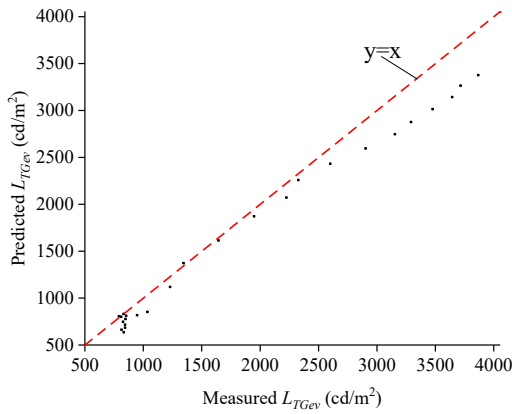


Fig. 8. Scatterplot of the measured L_{TGev} vs. the predicted L_{TGev}

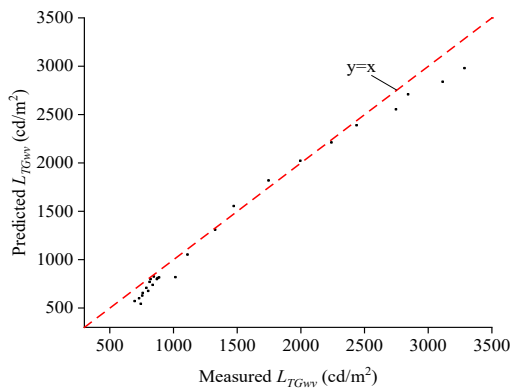


Fig. 9. Scatterplot of the measured L_{TGwv} vs. the predicted L_{TGwv}

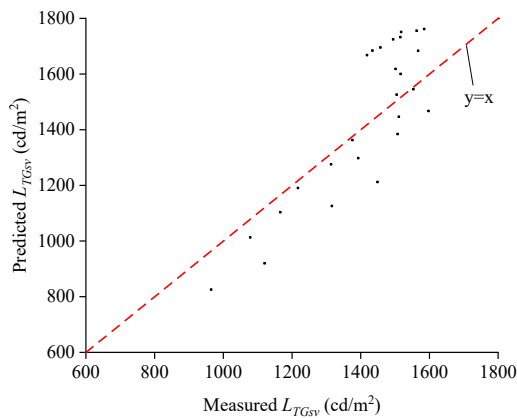


Fig. 10. Scatterplot of the measured L_{TGsv} vs. the predicted L_{TGsv}

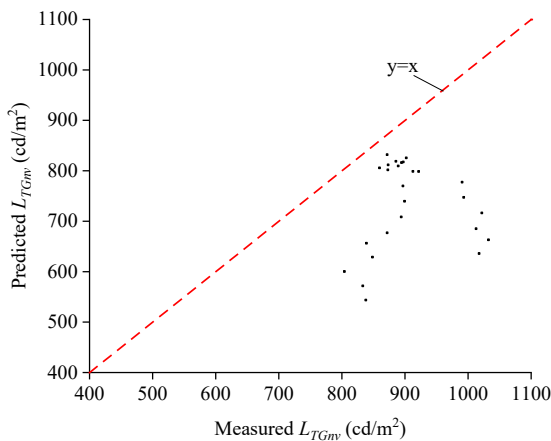


Fig. 11. Scatterplot of the measured L_{TGmv} vs. the predicted L_{TGmv}

Figures 12–16 show the relative error frequency distribution of L_R , L_{TGev} , L_{TGwv} , L_{TGsv} , and L_{TGmv} . The relative errors of L_R , L_{TGev} , L_{TGwv} , L_{TGsv} , and L_{TGmv} are -10% – 10% , -30% – 10% , -30% – 10% , -20% – 20% , and -40% – 0 , respectively. The relative error of L_R is the smallest, whereas the relative error of L_{TGmv} is the largest.

$$Relative\ error = \frac{(P - M)}{M} \times 100\% \quad (33)$$

where P denotes the predicted data, and M denotes the measured data.

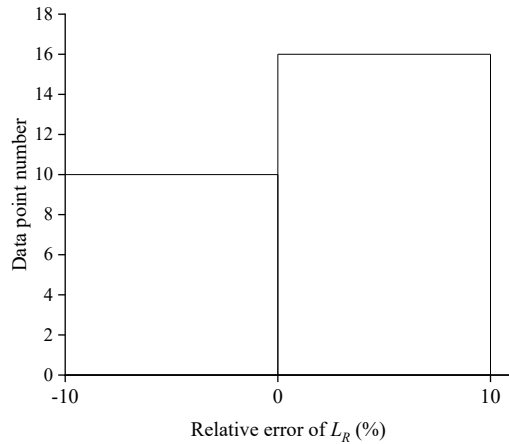


Fig. 12. Relative error histogram of L_R

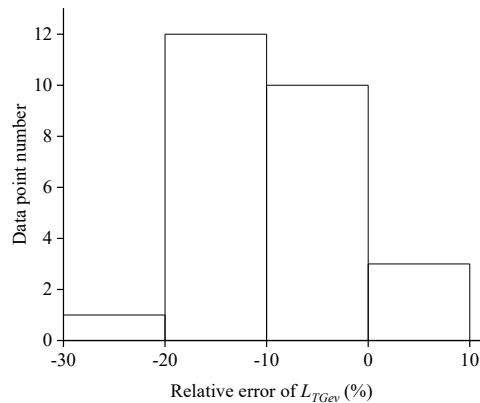


Fig. 13. Relative error histogram of L_{TGev}

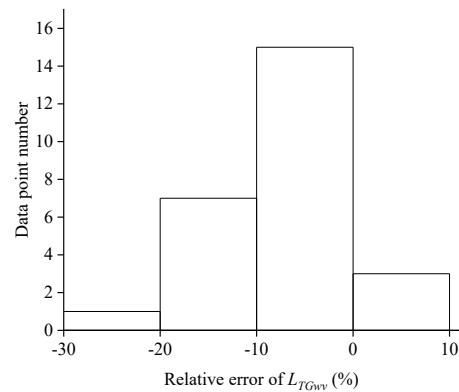


Fig. 14. Relative error histogram of L_{TGwv}

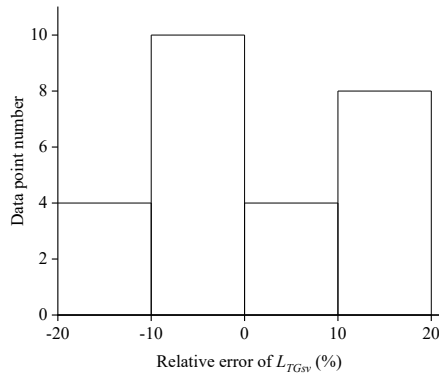


Fig. 15. Relative error histogram of L_{TGsv} .

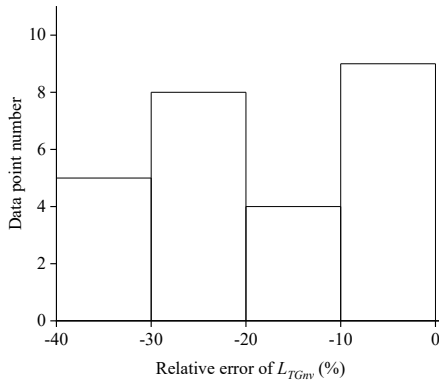


Fig. 16. Relative error histogram of L_{TGmv} .

The relative root-mean-square error (RRMSE) and relative mean bias error (RMBE) in statistics were used to evaluate the overall error of the forecast data. Table 5 shows the overall error of L_R , L_{TGev} , L_{TGwv} , L_{TGsv} , and L_{TGmv} . The RMBEs of L_{TGev} , L_{TGwv} , and L_{TGmv} are less than 0, indicating that the predicted values of L_{TGev} , L_{TGwv} , and L_{TGmv} are generally small. From Table 5, the overall error of L_R is the smallest, and that of L_{TGmv} is the largest. The measured L_R , L_{TGev} , L_{TGwv} , L_{TGsv} , and L_{TGmv} and the corresponding predicted values are generally in good agreement, indicating that the assumptions in Formulas 10–30 are appropriate.

$$RRMSE = \frac{\sqrt{\frac{\sum_{i=1}^n (P - M)^2}{n}}}{M} \times 100\% \quad (34)$$

where n is the amount of data, and \bar{M} is the average measured value.

$$RMBE = \frac{\sum_{i=1}^n (P - M)}{n \cdot \bar{M}} \times 100\% \quad (35)$$

Table 5. Overall error of object surface luminance

	L_R	L_{TGev}	L_{TGwv}	L_{TGsv}	L_{TGmv}
RRMSE (%)	5.4	13.5	9.1	11.2	22.2
RMBE (%)	1.8	-10.0	-6.4	2.0	-19.2

4.4 L_{20} verification

On May 29, 2020, L_{20} of the tunnel located at 104.41785 degrees east longitude and 31.090786 degrees north latitude (the time zone is the eighth zone of the eastern hemisphere) was measured. The sky was cloudless during the test. L_{20} test equipment was an imaging photometer (IC-PMY16, Radiant Vision Systems, Redmond, WA, USA). The tested tunnel portal was perpendicular to the asphalt pavement, and the azimuth that the portal faces was 257 degrees. The 20-degree field of view when the driver approached the tunnel is shown in Figure 17. The 20-degree field of view was divided into four different color areas, namely, light gray wall, black threshold zone, gray asphalt road, and tender green leaves. In accordance with the percentage of the four areas in the 20-degree field of view, L_{20} can be expressed as

$$L_{20} = 0.303L_R + 0.016L_{TG} + 0.013L_W + 0.668L_{th} \quad (36)$$

where L_{TG} is the luminance of the tender green leaves, L_W is the luminance of the light gray wall, and L_{th} is the luminance of the threshold zone.

Given that L_{th} is much smaller than the luminance of other areas and L_{th} can be ignored, Formula (36) can be simplified as

$$L_{20} = 0.303L_R + 0.016L_{TG} + 0.013L_W \quad (37)$$

The measured r values of the gray asphalt pavement, tender green leaves, and light gray wall are 0.072, 0.053, and 0.121, respectively.

The predicted value of L_{20} was compared with the measured value in Table 6 and Figure 18. Figure 19 presents that the relative error of L_{20} is 0–30%. The RRMSE and RMBE of L_{20} are 11.6% and 11.4%, respectively. The predicted L_{20} is slightly larger.

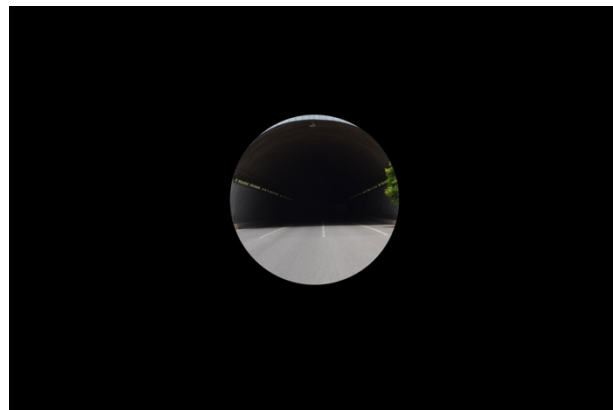


Fig. 17. 20-degree field of view

Table 6. Predicted and measured values of L_{20}

Time	Predicted L_R (cd/m^2)	Predicted L_{TG} (cd/m^2)	Predicted L_W (cd/m^2)	Predicted L_{20} (cd/m^2)	Measured L_{20} (cd/m^2)
13:00	8623	1058	2416	2661	2467
13:10	8593	1314	3000	2664	2452
13:20	8511	1558	3557	2650	2413
13:30	8388	1821	4158	2625	2351
13:40	8235	2026	4625	2588	2387
13:50	8060	2215	5056	2543	2303
14:00	7870	2389	5454	2494	2234
14:10	7670	2550	5821	2440	2245

14:20	7462	2699	6161	2384	2167
14:30	7248	2819	6436	2325	2102
14:40	7030	2953	6741	2265	1969
14:50	6809	3075	7021	2204	1975
15:00	6586	3188	7279	2141	1994
15:10	6361	3293	7518	2078	1829
15:20	6135	3390	7740	2014	1756
15:30	5908	3480	7945	1949	1741
15:40	5680	3564	8136	1884	1759
15:50	5451	3641	8312	1818	1588
16:00	5222	3712	8474	1752	1629
16:10	4993	3776	8622	1685	1487
16:20	4764	3834	8753	1619	1422
16:30	4535	3884	8868	1551	1437
16:40	4306	3926	8964	1484	1269
16:50	4077	3959	9038	1416	1205
17:00	3849	3980	9087	1348	1216
17:10	3621	3989	9108	1279	1060
17:20	3394	3984	9096	1210	989.6

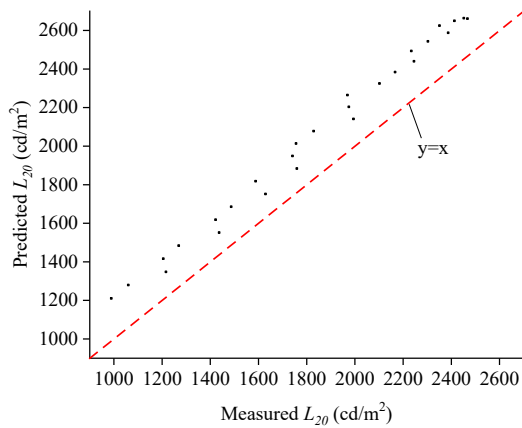


Fig. 18. Scatterplot of the measured L_{20} vs. the predicted L_{20}

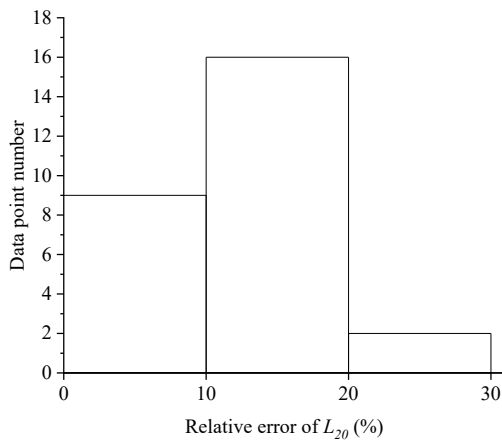


Fig. 19. Relative error histogram of L_{20}

4.5 Discussion

The proposed method can predict L_{20} of any time under a cloudless sky, whereas the CIE method can only obtain the maximum L_{20} in a year. The proposed method can predict L_{20} with portals with different inclination angles, whereas the CIE method does not consider the impact of the inclination of the portal on L_{20} . The CIE method is limited to obtaining L_{20} for four driving directions: east, west, south, and north. By contrast, the proposed method can predict L_{20} for any driving direction.

The largest potential error in predicting L_{20} comes from the prediction of $I_{\beta g}$. The used Perez point source model has two assumptions. One is that all the energy in the horizon zone is contained in an infinitely thin area with an elevation angle of 0 degree. The other is that all the circumsolar energy comes from one point. The above assumptions cause an error in predicting $I_{\beta d}$, especially when the surface cannot receive sunlight. but the Perez point source model is currently the most accurate model for predicting $I_{\beta d}$. The extraterrestrial irradiance and illuminance of the cloudless sky were assumed to reach the ground when the sun's altitude angle was 90 degrees in the used I_{hg}, E_{hg} model proposed by Liang et al.[19]. The above assumption causes small errors in the prediction of I_{hg}, E_{hg} . In addition, the values of f_l and f_g affect the accuracy of I_{is} and $I_{\beta r}$, respectively. All the above errors cause bias in $I_{\beta g}$.

Another source of error in predicting L_{20} is L obtained through $I_{\beta g}$. L within the 20-degree field of view is assumed to be the same at all viewing angles. Nevertheless, the objects in the 20-degree field of view reflect daylight approximately evenly in all directions. L is slightly distinct at different viewing angles.

The 20-degree field of view was divided into multiple areas of different colors to calculate L_{20} . The premise of the proposed L_{20} model is that the colors in the divided area are exactly the same. However, it can only be guaranteed that the colors in the segmented region are roughly the same when the 20-degree field of view is segmented, which causes errors in the predicted L_{20} .

5. Conclusions

This study proposed a new prediction model for object surface luminance to predict L_{20} of road tunnels under a cloudless sky. A combination of theoretical research and measured data was used. The predicted object surface luminance and L_{20} under a cloud-free sky were verified, and the reasons for the error were analyzed. In the end, the following conclusions were reached:

(1) Objects in the 20-degree field of view have approximately the same luminance at different viewing angles. It can be supposed that the ratio of luminance to illuminance on the surface of a specific color object is constant when predicting L_{20} . This ratio is not affected by the test time and weather, but the color is the decisive factor for the ratio.

(2) The proposed prediction method quantitatively considers all factors that affect L_{20} , such as weather, test time, the location of the tunnel, the inclination angle of the portal, the orientation of the portal, the color of objects around the portal, and the percentage of objects in the 20-degree field of view. The function cannot be achieved in the CIE method.

(3) In the example, the RRMSE and RMBE of L_{20} predicted using the proposed method are 11.6% and 11.4%, respectively, which can meet the engineering requirements.

L_{20} prediction method proposed in this study has good operability. The proposed method has reference significance

for intelligent dimming research of highway tunnels. CIE recommends 15 sky types. $I_{\beta g}$ is extremely difficult to predict under cloud sky types. The color, distribution, and thickness of clouds should be considered. This study only carried out L_{20} forecast of a cloudless sky. Predicting L_{20} under a clouded sky will be the focus of future research.

Acknowledgements

This work was supported by the National Natural Science Foundation of China. (Approval number: 51878107)

This is an Open Access article distributed under the terms of the Creative Commons Attribution License.



References

- Mavridou, T., Doulos, L. T., "Evaluation of different roof types concerning daylight in industrial buildings during the initial design phase: Methodology and case study". *Buildings*, 9(7), 2019, pp.170.
- Onaygil, S., Güler, Ö., Erkin, E., "Determination of the effects of structural properties on tunnel lighting with examples from Turkey". *Tunnelling and underground space technology*, 18(1), 2003, pp.85-91.
- García-Trenas, T., López, J., Peña-García, A., "Proposal to forest Alpine tunnels surroundings to enhance energy savings from the lighting installations. Towards a standard procedure". *Tunnelling and underground space technology*, 78(1), 2018, pp.1-7.
- Bouroussis, C. A., Nikolaou, D. T., Topalis, F. V., "Optimization of tunnel lighting control by re-aiming of the external L20 luminance meter". In: *CIE x046: 2019 Proceedings of 29th CIE Session*, Washington DC, USA: CIE, 2019, pp.1595-1604.
- Zhao, W., Liu, Q., Liu, S., Wang, Q., "Study on Time-varying Characteristics of Outside Brightness of Highway Tunnel". *Technology of Highway and Transport*, 33(5), 2017, pp.132-135.
- Wang, Y., Zhao, Y., Quan, Q., Cao, Z., "Dynamic characteristics of external luminance of highway tunnel in cold area". In: *IOP Conference Series: Earth and Environmental Science*, Dalian, China: IOP Publishing Ltd, 2020, pp.012024.
- Georgiev, V., "Optimization of Energy Consumption of Road Tunnels". In: *2020 Fifth Junior Conference on Lighting (Lighting)*, Ruse, Bulgaria: IEEE, 2020, pp.1-5.
- Peña-García, A., Salata, F., Golasi, I., "Decrease of the maximum speed in highway tunnels as a measure to foster energy savings and sustainability". *Energies*, 12(4), 2019, pp.685.
- Peña-García, A., Gómez-Lorente, D., "Installation of solar panels in the surroundings of tunnel portals: A double-targeted strategy to decrease lighting requirements and consumption". *Tunnelling and underground space technology*, 97(1), 2020, pp.103251.
- López, J., Peña-García, A., "Determination of lighting and energy demands of road tunnels using vehicle based photographs of the portal gates: An accessible and safe tool for tunnel renewal and maintenance". *Tunnelling and underground space technology*, 78(1), 2018, pp.8-15.
- Blaser, P., Dudli, H., "Tunnel lighting: Method of calculating luminance of access zone L20". *Lighting Research & Technology*, 25(1), 1993, pp.25-30.
- Pachamov, A., Pregyov, B., Kassev, K., "Annual use of luminaire groups for the entrance area according to the orientation of the road tunnel". In: *2019 Second Balkan Junior Conference on Lighting (Balkan Light Junior)*, Plovdiv, Bulgaria: IEEE, 2019, pp.1-4.
- Doulos, L. T., Sioutis, I., Tsangrassoulis, A., Canale, L., Faidas, K., "Revision of threshold luminance levels in tunnels aiming to minimize energy consumption at no cost: Methodology and case studies". *Energies*, 13(7), 2020, pp.1707.
- Xu, J., Wu, J., He, Y., "Discussion on Dynamic Characteristic of Road Tunnel Adaptation Luminance". *Lamps and lighting*, 42(1), 2018, pp.10-15.
- Deng, M., Zhang, F., "Method obtaining scenery luminance outside tunnel portals with in-situ testing". *Journal of civil, Architectural & Environmental Engineering*, 38(3), 2016, pp.118-122.
- Zhang, T., "Research of Determining Typical Elements' Luminance at Tunnel Portals By Radiation-Illuminance Conversion Method". Master thesis of Chongqing University, China, 2016, pp.49-77.
- He, W., Liang, B., "A Novel Method for Calculating Luminance in the Access Zone of a Road Tunnel based on a Digital Camera". *Journal of Engineering Science and Technology Review*, 14(3), 2021, pp.148 - 157.
- Xiao, Q., "Measurement of Tunnel Luminance and Vehicle Detection Based on Video Stream and its Application". Master thesis of Guilin university of electronic technology, China, 2018, pp.16-33.
- Liang, B., He, W., "Slope Illuminance Prediction under a Cloudless Sky Based on the Novel Model for Global Horizontal Irradiance and Illuminance". *Journal of Engineering Science and Technology Review*, 14(4), 2021, pp.135-145.
- Wu, Y., Liu, C., Wen, S., "Calculation of Sky Luminance Distribution at Arbitrary Time Based on the CIE Sky Model". *Acta Optica Sinica*, 34(11), 2014, pp.27-33.
- Perez, R., Seals, R., Ineichen, P., Stewart, R., Menicucci, D., "A new simplified version of the Perez diffuse irradiance model for tilted surfaces". *Solar Energy*, 39(3), 1987, pp.221-231.
- Perez, R., Ineichen, P., Seals, R., Michalsky, J., Stewart, R., "Modeling daylight availability and irradiance components from direct and global irradiance". *Solar Energy*, 44(5), 1990, pp.271-289.
- Darula, S., Kittler, R., Wittkopf, S. K., "Outdoor illuminance levels in the tropics and their representation in virtual sky domes". *Architectural Science Review*, 49(3), 2006, pp.301-313.
- Kittler, R., Darula, S., "Determination of sky types from global illuminance". *International Journal of Lighting Research and Technology*, 32(4), 2000, pp.187-193.
- Kittler, R., Darula, S., "Parametrization problems of the very bright cloudy sky conditions". *Solar Energy*, 62(2), 1998, pp.93-100.
- Darula, S., Kittler, R., "New trends in daylight theory based on the new ISO/CIE Sky Standard: 3. Zenith luminance formula verified by measurement data under cloudless skies". *Building Research Journal*, 53(1), 2005, pp.9-31.
- Meinel, A., Meinel, M., "Applied Solar Energy". Boston: Addison Wesley Publishing Co., America, 1976, pp.37-43.
- Ineichen, P., Perez, R., Seals, R., "The importance of correct albedo determination for adequately modeling energy received by tilted surfaces". *Solar Energy*, 39(4), 1987, pp.301-305.